

# First-principles investigation of the Ni-Fe-Al system

F. Lechermann<sup>a,1</sup>, M. Fähnle<sup>a</sup> and J.M. Sanchez<sup>b</sup>

<sup>a</sup>*Max-Planck-Institut für Metallforschung, Heisenbergstrasse 3, D-70569 Stuttgart, Germany*

<sup>b</sup>*Texas Materials Institute, The University of Texas at Austin, Austin, Texas, 78712, USA*

---

## Abstract

By combining ab-initio electron theory and statistical mechanics, the physical properties of the ternary intermetallic system Ni-Fe-Al in the ground state and at finite temperatures were investigated. The Ni-Fe-Al system is not only of high technological interest, but exhibits also rich physics, e.g., a delicate interplay between structure and magnetism over a wide composition range and substantial electronic correlations which is challenging for modern electronic structure methods. The new Stuttgart ab-initio mixed-basis pseudopotential code in the generalized gradient approximation (GGA) was used to determine the energetics in the ground state. Therewith, in combination with the cluster expansion (CE) method a representation of the energy landscape at  $T=0$  over the whole Gibbs triangle was elaborated. At finite temperatures, the cluster variation method (CVM) in tetrahedron approximation was employed in order to calculate the ab-initio ternary phase diagram on the bcc and fcc lattice. Thereby, a miscibility gap in the ternary B2 phase was theoretically verified.

*Key words:* NiAl, FeAl, Fe<sub>3</sub>Al, phase stability, density functional theory, Invar, ternary phase diagram

*PACS:*

---

---

*Email address:* Frank.Lechermann@cpht.polytechnique.fr (F. Lechermann).

<sup>1</sup> present address: CPHT École Polytechnique, 91128 Palaiseau Cedex, France.

# 1 Introduction

## 1.1 Theoretical background

From a theoretical point of view Materials Science can be understood as the study of the interplay between realistic many-body systems. Although a lot of simplified theoretical models to describe the physical properties of real materials work on a meso- or macroscopic level with coarse-grained variables, these models often exhibit badly defined materials parameters which stem from the true many-body problem. Thus, a microscopic ab-initio theory to model real materials systems is not only appreciated to shed light on the definition of such parameters, but also to provide a valuable tool to identify the important interactions and physical processes on an atomistic level that determine the macroscopic behavior. In recent years it became possible by the invention of effective approximations and the overwhelming increase of computer power to get a grip on the highly demanding calculational schemes of such microscopic modellings from first principles [1].

The ab-initio density functional theory (DFT) in the local-spin-density approximation (LSDA) and in the generalized-gradient approximation (GGA) is nowadays a widely accepted highly efficient method to describe the electronic structure of weakly correlated materials. In DFT the electronic many-particle problem in the ground state is exactly mapped on an effective single-particle formalism, whereby the many-electron wavefunction is replaced by the electronic charge density  $n(\mathbf{r})$  as the characterising quantity of the system [2,3]. In actual calculations only a small part of the total energy of the system, the exchange-correlation energy  $E_{xc}[n]$ , has to be approximated.

Due to the fact that in order to reveal the energetics of a given material system for arbitrary concentrations of the involved components a sole DFT description is still too costly, a suitable coarse-graining of the method has to be accomplished. This can be achieved in a well-defined way by the cluster expansion (CE) [4]. By this method, any function of the configuration on a given parent lattice can be expanded into cluster functions, whereby a cluster on the lattice is uniquely defined by the lattice points that are included in such a geometrical object. The CE coefficients are configuration independent. Through the structure inversion method (SIM) [5], a direct link between the CE and the ab-initio electron theory can be established by fitting the coefficients of the CE (terminated at a maximum cluster) to the ab-initio calculated data for the physical property which is to be cluster expanded. Because of the decoupling of expansion coefficients and occupations on the parent lattice, a CE established in such a way can be highly efficient in obtaining values for the physical quantity in question for arbitrary lattice configurations and arbitrary concentrations of the components. By construction, these new values should in principle have the same accuracy as those explicitly computed via

the underlying electronic structure method.

For the ab-initio description of finite temperature properties a modelling of the free energy of the material system has to be achieved. This can be done by including entropy in the cluster theory in the form of the cluster variation method (CVM) [6,7,4,8]. In the CVM one can write down a functional for the free energy where the internal energy is expressed by a CE with the cluster functions replaced by cluster correlation functions. The configurational entropy is also easily represented by the latter [4]. By minimizing the free energy functional with respect to the cluster correlation functions (or the cluster occupation probabilities which can also serve as natural variables in this problem) a meaningful approximation to the true free energy of the system can be obtained. The approximation is of course given by the limited number of clusters one can consider in the practical cluster theory. In the limit of the inclusion of all possible clusters, the CE and the CVM become mathematically exact on a given parent lattice.

## 1.2 The Ni-Fe-Al system

The present first-principles investigation was carried out for the ternary intermetallic system Ni-Fe-Al. Most of this type of modelling was done in the past for binary systems, only few such ab-initio assessments can be found in literature for ternary or even higher multicomponent materials systems. This is in contrast to the technological development of new materials, where in most cases more than two components are necessary to attain desired materials properties. As an example for this serve alloys which are based on Ti, Fe and Ni aluminides [9]. Structural alloys derived from these intermetallic phases are promising candidates for high performance materials, because they show high strength at all temperatures, low density and high chemical resistance. The main drawback of these aluminides is their brittleness, in particular at low temperatures. To overcome this drawback and also to further improve the advantageous materials properties, either substitution of atoms by impurities or addition of other phases to the given one have to be considered. For instance, small additions of Boron to Ni<sub>3</sub>Al have a ductilization effect [10]. Concerning NiAl, it was found that minor amounts of Fe additions also enhance the ductility [11]. Furthermore, as shown by Letzig *et al.* [12] the complete Ni-Fe-Al system offers various alloying possibilities for softening NiAl and Ni<sub>3</sub>Al, too. But a theoretical investigation of this ternary system may be motivated not only from a purely technological point of view. Besides the general need for consolidation of the first-principles alloy theory for multicomponent systems, i.e., higher than binary, the Ni-Fe-Al system exhibits also rich physics from a very fundamental point of view. The system incorporates two transition metals, Ni and Fe, with partially filled *3d* states which can give rise to localized electronic behavior, and the simple metal Al with itinerant *s* and *p* states.

Moreover, Ni and Fe are ferromagnetic in their elemental crystal ground state, whereby the structure differs, i.e., Ni crystallizes on a fcc and Fe on a bcc lattice. Nonmagnetic Al is again stable in a fcc structure, but with a much larger lattice constant compared to fcc-Ni, since the atomic radius of Al is 15% bigger than the atomic radius of Ni (Ni and Fe atoms have nearly identical atomic radii in the solid state). Therefore, depending on the concentration of the three constituents, a strongly varying behavior in the electronic structure, magnetism and the alloy structure is expected. Already well studied are the binary subsystems, i.e., Ni-Fe, Ni-Al and Fe-Al (see [13,14,15] and references therein). The Ni-Fe system, with the famous Invar region [16] around  $\text{Ni}_{35}\text{Fe}_{65}$ , shows a very strong influence of magnetism on the phase stability. In contrast, in Ni-Al this influence is nearly negligible. Lying between these limiting cases, Fe-Al shows a very delicate interplay between structure and magnetism [15,17,18,19]. In addition, the Al-rich aluminide systems exhibit low ordering energies that give rise to stable crystal structures with low symmetries, whereas for the transition-metal-rich regions only structures on the bcc and fcc lattice are stable.

Only very few theoretical approaches to model Ni-Fe-Al are known from literature (e.g., [20,21]). Especially, there exists no complete theoretical description for the global system, also not with empirical parameters. There are experimental investigations (for instance, [22,23] and references therein), but the overall understanding of this system, in particular on an atomistic level, is rather scarce. Hence the present work is dedicated to provide an introduction to an ab-initio modelling of Ni-Fe-Al by revealing some insight in the interesting physics of this system.

## 2 Computational procedure

### 2.1 DFT calculations

To elucidate the ground state properties of Ni-Fe-Al, as a first step DFT calculations with our ab-initio mixed-basis pseudopotential (MBPP) code [24] were performed for chosen reference solid compounds. In the MBPP code, norm-conserving pseudopotentials are used and the basis consists of plane waves and a few additional localized functions per atom. For  $E_{xc}$  we used the GGA given by Perdew, Burke and Ernzerhof (PBE) [25]. In the whole modelling only structures on the bcc and fcc lattice were taken into account (with a small exception for Al-rich Ni-Al at  $T=0$ , cf. section 3.1.2), thereby restricting the Ni-Fe-Al system onto these cubic parent lattices. As other lattice types become important only in the technologically less interesting Al-rich region of the ternary phase diagram [22,23], this restriction cuts off only a small part of common general interest. To investigate the influence of collinear magnetism

we performed both spin-unpolarized and spin-polarized calculations for each considered crystal structure.

In the MBPP calculations, the numbers of k-points in the irreducible wedge of the 1. Brillouin zone were 408, 440 and 280 for fcc-Ni, bcc-Fe and fcc-Al, respectively, in order to ensure an equivalent k-point grid for the different structures. With the same intention, the k-point grid for all the treated compounds was chosen in such a way that the density of sampled k-points was the same for each structure. The cut-off energy for the plane waves was generally set to 24 Ryd, and throughout the calculations a Gaussian smearing of 0.05 eV was employed. With this choice for the convergence parameters the relevant formation energy  $E_f$ , defined for a given structure  $\sigma$  as

$$E_f(\sigma) = E_{tot}(\sigma) - c_{\text{Ni}}E_{tot}^{(\text{fm})}(\text{fcc-Ni}) - c_{\text{Fe}}E_{tot}^{(\text{fm})}(\text{bcc-Fe}) - c_{\text{Al}}E_{tot}^{(\text{nm})}(\text{fcc-Al}), \quad (1)$$

with the concentration  $c_i$  of the species and the total energy  $E_{tot}$ , whereby the superscripts 'nm'/'fm' indicate the nonmagnetic/ferromagnetic state, can be converged to 0.05 meV/atom.

## 2.2 Cluster expansions

From the calculated formation energies and magnetic moments, a set of CEs was constructed via the SIM. In practise, a CE for the function  $f$  of the configuration  $\sigma$  in an  $M$  component system on a given parent lattice can generally be written as [4]

$$f(\sigma) = f_0 + \sum_{\alpha, m}^{\gamma, M-1} f_{\alpha m} \phi_{\alpha m}(\sigma_\alpha) \quad , \quad (2)$$

where  $\phi_{\alpha m}$  is the cluster function for cluster  $\alpha$  and degree  $m$ ,  $f_{\alpha m}$  is the cluster expansion coefficient and  $\gamma$  is a maximum cluster. The quantity  $f_0$  designates the empty cluster. The cluster function is suitably chosen to be a function of spin variables  $\sigma$ . For the considered ternary case values of 1, -1 and 0 were attributed to these occupation variables assigned to Ni, Fe and Al. As the complete ternary basis for the cluster functions  $\phi_{\alpha m}$ , we used  $\Theta_1 = \{1, \sigma, \sigma^2\}$ , and for comparison also the orthonormal Chebychev basis [4,26], below named  $\Theta_2$ . The clusters  $\alpha$  belong to a chosen set with a maximum cluster  $\gamma$ , where  $\alpha$  does not necessarily have to be a subcluster of  $\gamma$ . The expansion coefficient  $f_{\alpha m}$  will be named  $K_{\alpha m}$  in the case of the formation energy. Note that generally any CE coefficient can be understood as an effective cluster interaction (ECI) which includes contributions from physical interactions within and outside the cluster range [27].

In our work, CEs for the bcc and fcc lattice were constructed. Two cluster sets were used. First, we extracted for both parent lattices a traditional tetrahedron CE (T-CE) (see [28] and references therein) from the ab-initio calculated data

for the physical quantities in question, i.e., formation energy and magnetic moment, of selected reference configurations. In this T-CE, all used clusters are subclusters of the minimum tetrahedron on the given lattice. On the bcc lattice this includes 5 clusters, namely the point, the nearest-neighbor (NN) pair, the next-nearest-neighbor (NNN) pair, the triangle with two NN pairs and one NNN pair and the irregular tetrahedron itself with two NN pairs and two NNN pairs. For the fcc lattice the T-CE corresponds to 4 clusters, i.e., the point, the NN pair, the triangle with three NN pairs and the regular tetrahedron with four NN pairs. Hence, whereas the bcc T-CE incorporates NNN correlations, the fcc T-CE includes only NN correlations. Due to the completeness requirement, there are 21 cluster functions on the bcc lattice and 15 on the fcc lattice in the ternary case for the tetrahedron approximation. The same numbers of ECIs were determined by the SIM via matrix inversion, i.e., the number of reference structures was equivalent to the number of ECIs.

As we were mainly interested in the ternary B2 phase of the Ni-Fe-Al system, we developed in addition a higher CE for the bcc lattice with 13 clusters, including the point, pairs up to the 6th NN, four triplets, the irregular tetrahedron and a pentahedron (s. Fig. 1). It follows that there are 65 different cluster functions, and associated therewith, of course, the same number of ECIs, for the ternary system. In that case the SIM was performed via a least-mean-squares fit of 127 ab-initio calculated formation energies and magnetic moments, out of which 75 belonged to binary and 49 to ternary compounds. We will name this CE, according to the maximum body cluster, 'pentahedron CE (P-CE)' but note that in contrast to the T-CE, this does not mean that all and only the subclusters of this pentahedron are included.

With these cluster sets, the formation energy and the magnetic moment were expanded in different schemes. First, the spin-unpolarized and spin-polarized formation energy were expanded for both parent lattice types with allowing only for global volume relaxations but no structural relaxations of the reference structures, in order to reveal the influence of magnetism in the fixed geometries. Thereby, as an approximation we allowed only for ferromagnetic (fm) alignment of the local moments which possibly develop in the spin-polarized MBPP calculations. This can be validated by the experimental observation that all stable cubic ordered compounds in the Ni-Fe-Al system are ferromagnetic in their respective ground state when showing magnetic behavior. The only critical case is stoichiometric FeAl, where DFT in LSDA/GGA predicts a ferromagnetic ground state [17], whereas experimentally no net magnetic moment at very low temperatures is detected [29]. Throughout the rest of the paper the nomenclature  $E_f^{(\text{fm})}$  will be used for the cluster-expanded formation energies of structures with potentially ferromagnetic order, i.e., the magnetic energy is implicitly included in that CE.

Additionally, we checked for the influence of "local structural relaxations" on the bcc lattice by cluster-expanding also the spin-polarized formation energy for the structurally relaxed reference structures. During a "local structural relaxation" all atoms are relaxed but the unit cell is kept cubic, i.e., no shape

relaxation of the supercell is performed. For instance, among the various considered configurations in the supercell there are such which would lead to a tetragonal distortion of the supercell if we allowed for a  $c/a$  relaxation. To keep the cubic shape of the supercell during structural relaxation seems to be meaningful for a modelling with multiple parent lattices, as employed here. Within a “full structural relaxation” including shape relaxation, the connection between the reference structure and its supposed parent lattice may get lost more easily. An example is the case of tetragonal  $L1_0$ -NiAl on the fcc parent lattice, which transforms into B2-NiAl on the bcc parent lattice when relaxing  $c/a$  [30]. The described way of including the structural relaxations was performed only in the more sophisticated pentahedron approximation. Throughout the rest of the paper, the resulting CE is correspondingly named rP-CE.

The mean error in meV/atom for the ECIs from the least-mean-squares fitted SIM was 13.4, 11.1 and 12.0 for the spin-unpolarized P-CE, the spin-polarized P-CE and the rP-CE (spin-polarized) in the  $\Theta_1$  basis, respectively. Hence, the latter CEs should be well enough converged to account for a meaningful description of the energetics in the given approximations.

In order to investigate the relevant energy landscape of Ni-Fe-Al by the constructed ternary CEs, we developed a simple algorithm to determine homogeneous lowest-energy structures for each given ternary composition. In this algorithm, a random starting configuration is successively modified by site exchange of, respectively, two atoms in a periodically continued supercell. After each such Monte-Carlo sweep, the energy of the new structure is calculated and the structure will be accepted if the energy is lower than the one of the old structure. For the supercells, sizes of 54 and 108 atoms were used in the calculations. The minimum formation energy is usually reached in some thousand sweeps and the corresponding optimized homogeneous structure may be extracted. Please note that the so obtained homogeneous lowest-energy structures for arbitrary compositions are not necessarily identical to the true ground state structures which are often heterogeneous mixtures of various phases.

### 2.3 CVM calculations

For the calculation of the ternary incoherent phase diagram on the bcc and fcc lattice at finite temperatures, the CVM in tetrahedron approximation was employed for the internal energy and the configurational entropy. The ab-initio ECIs  $\{K_{\alpha m}^{\text{tm}}\}$  obtained from the spin-polarized MBPP calculations were used for the representation of the internal energy. By confining to ferromagnetic order in the MBPP calculations the effect of thermal magnetic excitations on the finite temperature phase diagram is neglected. The actual CVM calculations were performed in a grand canonical ensemble with the set of effective chemical potentials  $\{\tilde{\mu}_{Ni}, \tilde{\mu}_{Fe}, \tilde{\mu}_{Al}\}$  and the effective grand potential  $\Omega(T, V, \{\tilde{\mu}_i\})$ ,

whereby the CVM equations were solved by the Natural Iteration Method (NIM) [31]. This whole procedure is described in detail elsewhere [32]. Although vacancies are in principle important defects in phase diagram calculations of intermetallic aluminide systems [33], they were not taken into account in this investigation. In a coherent modelling, this would call for a quaternary description with the vacancy as a fourth component with chemical potential zero. Also, vibrational effects on the thermodynamics were neglected.

### 3 Results

#### 3.1 Zero temperature

##### 3.1.1 General remarks

In the Tabs. 1 and 2 the structural data for the structures on the bcc and fcc parent lattice used for the development of the respective CEs in tetrahedron approximation, i.e., T-CEs, are shown. All structures correspond to a specific tetrahedron occupation on the respective parent lattice [28], hence these compounds have a small unit cell and order in NN and NNN neighbor distances. The first line for each compound in Tabs. 1 and 2 corresponds to a spin-unpolarized calculation, the second line to a spin-polarized one with possible fm order. The lattice constants are generally increased and the bulk moduli are decreased by ferromagnetism. The compounds with a '\*' are confirmed ground states in the Ni-Fe-Al system [23]. Thus, none of the highly ordered fully ternary structures are stable within the temperature regime investigated in experiment. From our MBPP calculations the necessary condition for phase stability, i.e., a negative formation energy, is fulfilled by all these structures, at least when taking into account ferromagnetism. However, by checking the possible tie line constructions [34] within the given set of reference structures, we can confirm the experimental observation from the  $T=0$  viewpoint, although the case of NiFeAl<sub>2</sub> is delicate (more on this stoichiometry in section 3.1.3). The CE of the possibly ferromagnetic compounds accounts implicitly for the magnetic degrees of freedom. Thereby it is assumed that these degrees of freedom are strongly coupled to the chemical degrees of freedom which are treated explicitly in Eq. (2). Furthermore, as already mentioned, other spin orderings were not allowed, and concerning the energy it was assumed that the energies of such possible non-fm configurations can be approximated by the fm energy contribution. Both approximations might be critical in some regions of the Ni-Fe-Al phase diagram, e.g., the Invar region in Ni-Fe [35], but should be reliable for a qualitative inspection of the general trends in the whole system.

The ECIs for the CEs of the formation energy in tetrahedron approximation



are shown in Tab. 3 for the nonorthogonal  $\Theta_1$  and the orthonormal  $\Theta_2$  basis. Although both sets of ECIs stem from an exact SIM with the same reference structures, the decay of the absolute value of the ECIs is generally more clearly visible within the  $\Theta_2$  basis. However, in practical convergence tests via the prediction of energies of new structures not included in the SIM, no appreciable differences between the two basis sets were observed (for a further discussion on this matter see, e.g., [26]).

The discussion of the ECIs in a ternary system is not as straightforward as in the binary case, because due to the completeness relation of the CE there are now multiple interactions associated with each geometrical cluster. A first estimation of the ordering/segregation behavior is, for instance, not easily connected to the sign of the effective pair interactions (EPI) from the common CE [26]. Thus, in order to illustrate this behavior it is more appropriate to map the obtained ternary EPIs onto effective quasibinary pair interactions  $W_{NiFe}^{(n)}$ ,  $W_{NiAl}^{(n)}$  and  $W_{FeAl}^{(n)}$  [26], where  $n$  denotes the near neighbor distance, that again yield a first information about the ordering/segregation behavior of the system via their sign. Thereby, positive (negative) values describe ordering (segregation) behavior. The values for these quasibinary EPIs, obtained from a mapping of the ternary EPIs from Tab. 3, are shown in Tab. 4. It is seen that the  $W^{(n)}$  between the transition-metal atoms and the Al atoms are always of an ordering type, in the case of  $W_{FeAl}^{(n)}$  subtly influenced by magnetism. In contrast, the NiFe interactions on the bcc lattice remain negative in NN distance even when ferromagnetism (very important in the binary Ni-Fe system, see Tab. 1) is taken into account. Only on the fcc lattice with ferromagnetism there is a indication for weak ordering tendencies. Although the NN pair interactions seem to be dominant in Ni-Fe-Al, of course, the effect of the multiplet and also of the higher pair interactions beyond NNN distance is neglected in the simple set  $\{W_{AB}^{1,2}\}$ .

### 3.1.2 Binary subsystems

For the whole composition range, Fig. 2 shows the ferromagnetic formation energy and magnetic moment for homogeneous periodic configurations of the binary subsystems of Ni-Fe-Al at zero temperature. In Fig. 2a the MBPP formation energies for the binary "canonical" tetrahedron-representable ordered structures from Tab. 1 and 2 are depicted. Additionally, for Ni-Al the formation energies of the noncubic experimentally stable structures  $D0_{11}$ -NiAl<sub>3</sub>,  $D5_{19}$ -Ni<sub>2</sub>Al<sub>3</sub> and "Ga<sub>3</sub>Pt<sub>5</sub>"-Ni<sub>5</sub>Al<sub>3</sub> are also included. The latter structures were structurally relaxed within the MBPP code, whereas the canonical structures are cubic structures (apart from the ones with  $L1_0$  symmetry) for which no structural relaxation degrees of freedom exist. The  $L1_0$  structures were restricted to the fcc parent lattice (see section 2.2). The ground state structures according to the MBPP calculations are connected with straight lines in Fig. 2a. For Ni-Fe,  $L1_0$ -NiFe was also theoretically verified as a stable ground state

structure within the investigated set, although experimentally this is still questionable [13]. In the Ni-Al system the correct ordered ground states according to experiment are obtained, except for “Ga<sub>3</sub>Pt<sub>5</sub>”-Ni<sub>5</sub>Al<sub>3</sub> which we were not able to verify as a stable ground state structure (also when including structural relaxations). Problematic seems to be the case for Fe-Al, as in PBE-GGA the important D0<sub>3</sub>-Fe<sub>3</sub>Al structure was not identified as the stable ground state at Fe<sub>75</sub>Al<sub>25</sub>, but L1<sub>2</sub>-Fe<sub>3</sub>Al. This seems to be due to the subtle electronic structure in this region of Fe-Al, where simple approximate exchange-correlation functionals, i.e., LSDA and GGA, might be not appropriate. For a discussion of this peculiarity see [18,19].

The zero temperature description according to the CEs constructed from the reference structures including spin-polarization, shown in Fig. 2b, yields important additional information. The lines in Fig. 2b correspond to the curves of lowest formation energy for the homogeneous structures obtained from the Metropolis-inspired algorithm described at the end of section 2.2. To obtain these curves, a homogeneous structure optimization for 26 concentrations in the interval [0,1] was performed with this algorithm, and the minimum formation energy was extracted, respectively. First, the formation energy in Fig. 2b shows for Ni-Fe major energy differences between phases on the bcc and the fcc parent lattice. The energetical crossover lies just around the Invar region. One can also see the important change in the sign of  $E_f^{(\text{fm})}$  for structures on the bcc lattice from positive to negative when applying the pentahedron CEs, especially for the Fe-rich system. However, the corresponding phases are metastable because their formation energies lie above the connecting line between the ground state structures bcc-Fe, L1<sub>0</sub>-NiFe, L1<sub>2</sub>-Ni<sub>3</sub>Fe and fcc-Ni. The magnetic moments of these metastable phases are substantially enhanced, as seen by the maximum in the corresponding curves in Fig. 2c. Turning over to Ni-Al, the large negative formation energy curves in this system exhibit a strong symmetry with respect to the equiatomic composition. These energies show a similar qualitative compositional dependence on both cubic parent lattices, whereby the bcc lattice is favoured around the equiatomic composition. The D0<sub>11</sub>-NiAl<sub>3</sub> phase lies obviously in the bcc/fcc transition region, the same applies for the Ni<sub>5</sub>Al<sub>3</sub> stoichiometry (see also [36]). Although our calculations do not stabilize “Ga<sub>3</sub>Pt<sub>5</sub>”-Ni<sub>5</sub>Al<sub>3</sub>, the large relaxation energy around this composition yields a hint for a possible martensitic transition. In general, the magnetic energy does not seem to be essential, although in the Ni-rich region it has some influence which can be relevant for the phase stability [37]. The increase of the magnetic moment with increasing Ni content is also clearly seen in Fig. 2c. Finally, it is apparent from the figure that the energetical competition between the bcc and fcc parent lattice becomes most delicate for the case of Fe-Al. The formation energy curves for both lattice types are very similar over a wide composition range. Also, the relaxation energy appears to be crucial in determining the correct phase stability. Especially around the equiatomic composition, the differences between the various approximations are significant. In contrast to Ni-Al, the magnetic moment persists in the Al-

rich region of Fe-Al and may have relevant influence on the already sensitive energy landscape. As already stated, the existence of a net magnetic moment at equiatomic FeAl is experimentally not verified, but the sensitivity to magnetic degrees of freedom is nevertheless experimentally confirmed [38], also for larger Al content [39].

### 3.1.3 Ternary system

Turning now to the multicomponent system, Fig. 3 shows lowest formation energy landscapes for ternary Ni-Fe-Al in the Gibbs triangle representation. These landscapes were computed again via our algorithm to find the minimum formation energy utilizing the respective CEs. Therefore, we introduced a 2-dimensional mesh of 338(254) grid points for the bcc(fcc) parent lattice inside the Gibbs triangle. At each of these grid points we searched for the homogeneous phase with the lowest formation energy within a given periodically continued supercell. Please recall that in this kind of calculations we again did not perform any tie line construction to account for heterogeneous phases, which would result in a true ground-state phase diagram.

On both cubic parent lattices, the respective minimum formation energy is nearly exclusively negative inside the Gibbs triangle. Only close to the binaries or to the pure elements,  $E_f^{(\text{fm})}$  reaches positive values in selected cases. The topology of the formation energy landscape appears to be very similar on the two parent lattices. Generally,  $E_f^{(\text{fm})}$  exhibits the largest negative values around the region with 50% Al, with a deep valley leading towards the  $\text{Ni}_{50}\text{Al}_{50}$  composition (Fig. 3a). Important information concerning the relative stability of the two cubic parent lattices is provided by Fig. 3b which displays the difference between the obtained formation energies for phases on the bcc and the fcc lattice. Clearly seen is that the phases on the fcc lattice dominates the Ni-rich and the Al-rich region of Ni-Fe-Al. The range where the homogeneous phases on the bcc lattice have lower formation energy than those on the fcc lattice resembles a belt shape, oriented along Fe-NiAl. Thereby, two stability centers may be identified. One is located at NiAl and the other distinct one is centered at the Fe corner of the triangle. The bridge between these centers becomes very fragile around the  $\text{NiFe}_2\text{Al}$  composition, indicating a strong competition with phases on the fcc lattice in this region. This competition was already experimentally verified in early studies of the Ni-Fe-Al system (see [22] and references therein). The nearby problematic  $\text{Fe}_3\text{Al}$  section (see section 3.1.2) underlines the delicate energetics in this area. Regarding the influence of ferromagnetism on the formation energy (see Figs. 3c,d), it is obvious that the main magnetic energy contributions arise for Fe-rich alloys. On the fcc lattice, the magnetic energy contribution exhibits maxima around NiFe and  $\text{Fe}_3\text{Al}$ , whereas on the bcc lattice one deep funnel centered at the Fe corner appears. In general, the behaviour of the cluster-expanded fm moment follows mainly the one of the magnetic energy over the Gibbs triangle.

Although the influence of magnetism is manifest in the Fe-rich region, even for compositions without a dominant fraction of Fe the magnetic energy gain for a wide range of alloys is still larger than 50 meV/atom. Hence, a neglect of this important energy term could lead to a qualitatively wrong picture of the Ni-Fe-Al system. Finally, we checked for the importance of higher cluster correlations on the bcc lattice. Fig. 3e shows the difference between  $E_f^{(\text{fm})}$  in tetrahedron and in pentahedron approximation. Additionally, in Fig. 3f the relaxed pentahedron approximation (rP-CE) was utilized to calculate this difference. One can observe that the tetrahedron approximation is not too bad for the bcc stability region. Deviations of the order of  $\pm 20$  meV/atom are surely comparable to the underlying DFT-GGA errors. Significant impact of the higher correlations appears for the Ni-rich, and by turning on the effect of structural relaxations, also for the Al-rich region. In both cases the higher cluster correlations tend to further lower the optimal formation energy. This effect is intuitively clear for the Al-rich region because of the different atomic sizes of the transition metal atoms and the Al atom. By structural relaxations, the system can reduce internal stress by lifting the constraints for the atomic positions imposed by the unperturbed parent lattice. Generally, for structures with cubic symmetry the ordering energy is small in the Al-rich region. The energy gain for Ni-rich bcc-alloys by taking into account larger clusters might be due to the fact that the bcc parent lattice is not energetically favorable in this region. The larger clusters stabilize structures with bigger unit cell, for which the locally defined “bcc character” diminishes. In other words, the stabilization of large unit cells against small unit cells indicates a low ordering energy on the given parent lattice. Recall that Ni-rich Ni-Fe-Al belongs to the region where phases on the fcc lattice are energetically favorable.

In order to quantify the predictive power of our ternary CEs, we present at the end of these  $T=0$  considerations a ground state investigation for the  $\text{NiFeAl}_2$  composition. Remember that our Metropolis-inspired algorithm determines the lowest-energy ordered structure for a given composition. However, this structure is only stable if in the diagram of the formation energy vs. composition its formation energy lies below the tie line connecting the formation energies of at least two neighbouring phases. Otherwise, a heterogeneous mixture of the corresponding phases is thermodynamically more stable than the homogeneous phase. When we want to check for a ternary system the stability of the lowest-energy ordered structure for a given composition, we in principle have to investigate the position of its formation energy relative to the tie lines corresponding to all possible neighbouring phases in all directions of the Gibbs triangle [34]. Because this is very time-consuming, after checking the energetics of the binaries, i.e., Figs. 2a,b, we confined the detailed study to the NiAl–FeAl quasibinary. As from the latter check, due to the strongly negative formation energy of B2-NiAl and B2-FeAl, phases on the NiAl–FeAl quasibinary line appear to be the most promising competitors against an homogeneous phase at  $\text{NiFeAl}_2$ . Note that the NiAl–FeAl line also serves as a boundary for the importance of ferromagnetism with increasing

Al content (see Fig. 3c), i.e., ordering tendencies along this line are also interesting from that point of view. From experiment, no ordered structure is known for NiFeAl<sub>2</sub>. In Fig. 4a the formation energies along NiAl–FeAl according to the different CEs are plotted. First, the fcc T-CE yields a noticeably higher formation energy curve than the simple B2-NiAl–B2-FeAl tie line, i.e., the fcc parent lattice provides no promising candidates concerning an ordered ground state. Turning to the bcc lattice, the  $E_f^{(\text{fm})}$  curve belonging to the T-CE is nearly identical to the straight B2-NiAl–B2-FeAl tie line, and the simple Heusler L2<sub>1</sub> structure (see Fig. 5a) is nearly pinned to this line (the other canonical bcc structure with symmerty F $\bar{4}$ 3m lies much higher in energy). On the other hand, the  $E_f^{(\text{fm})}$  curves originating from the pentahedron CEs run clearly below the B2-NiAl–B2-FeAl tie line and display a convex behavior close to NiFeAl<sub>2</sub>. Hence from the latter, an ordered ground state seems likely at this stoichiometry. Two structures, here named “G1” and “G2” (see Fig. 5b,c), found by means of the higher pentahedron CEs, are located in the favourable energy range. Actually, the G1 structure was identified as stable within a first higher cluster approximation beyond the tetrahedron approximation. By refining the CE into the final P-CE, now with G1 belonging to the set of input structures of the respective SIM, we finally obtained the G2 structure as the stable ordered structure for this composition. Tab. 5 lists the relevant data for the competing structures at NiFeAl<sub>2</sub>. The structures found from the CE investigation are by construction fixed on the rigid bcc parent lattice, since in the CE the total energy including the relaxation energy is represented as a function of configurations on the undistorted parent lattice. In reality, the structures G1 and G2 possess tetragonal symmetry, and only for the G2 structure no forces appear in the bcc configuration. The G1 structure consists of alternating [100] Ni, Al and Fe planes. When actually relaxing G1 within the MBPP code, the Al planes are shifted towards the Fe planes. Still, structurally relaxing the G1 structure does not shift its formation energy below the value for G2 within the full electronic structure method. The corresponding formation energies obtained via the P-CE and rP-CE are very close to the MBPP reference values and one yields the same energetic hierarchy between the structures, showing the quantitative reliability of the constructed CEs. Concerning the curvature of the P-CE and rP-CE minimum formation energy curves, the overall progression between NiAl and FeAl excludes a tie line construction that destabilizes the G2 structure. Moreover, it appears that at  $c_{\text{Fe}}=0.125$  there might be another pronounced ordering tendency, indicated by a convex kink in the P-CE and rP-CE curves. This opens the possibility for an additional ordered state at Ni<sub>3</sub>FeAl<sub>4</sub> within the given constraints. Concerning the behavior of the magnetic moment, the situation is delicate. As in DFT LDA/GGA ordered B2-NiAl is nonmagnetic and ordered B2-FeAl shows ferromagnetism, an onset of the latter must appear on the NiAl–FeAl line. From the CE calculations, already close to B2-NiAl a fm moment should be expected. On the contrary, the MBPP calculations reveal no resulting magnetic moment for G1 and G2. Interestingly, close to the FeAl stoichiometry

the magnetic moment strongly differs for different CEs. The complex interplay between structure and magnetism in the FeAl region is thus again manifest.

### 3.2 *Finite temperature phase diagram*

In this last section we want to discuss our result for the ternary Ni-Fe-Al phase diagram at finite temperature, investigated within the CVM using the ab-initio ECIs for the energetics. The full ternary phase diagram is the result of the interplay of a large number of different mutually coupled degrees of freedom. Because of the complexity of the problem we had to adopt approximations on several levels. For completeness, we like to list these approximations in the following.

- a. For the Fe-rich part of the phase diagram there is a very delicate interplay between electronic correlations, magnetism and structure [29,15,16,35,19], and for an accurate description of some of the binary Fe-Al subsystems it seems that one has to go beyond the LDA/GGA to the exchange-correlation energy of the DFT. In order to make the calculations for the whole ternary phase diagram feasible, we nevertheless adopted PBE-GGA for the construction of the ECIs.
- b. We take into account the effect of magnetism by allowing for a possible fm alignment of the magnetic moments, but the effect of thermal magnetic excitations is neglected.
- c. We take into account the configurational entropy within the CVM, but the contributions of phonons and single-electron excitations to the free energy are neglected.
- d. The effect of vacancies is neglected although vacancies are, at least, important for the Ni-Al phases on the bcc parent lattice [33].
- e. There are a few complex low-symmetry phases existing in the Al-rich part of Ni-Fe-Al. We, however, allow only for phases on a bcc or fcc parent lattice.
- f. For the internal energy and the entropy we employed the tetrahedron approximation on the bcc and fcc parent lattice to the CVM. This allows us to consider only phases with up to four sublattices [32].
- g. Due to the short range and the small number of degrees of freedom in the tetrahedron approximation, it seems not meaningful to include effects of local atomic relaxations, albeit they are surely important. Hence we did not include such effects which would require to consider a correspondingly enlarged set of reference structures in a least-mean-squares fitted SIM.

In view of these approximations we can not expect to be able to describe all the details of the physics of the ternary phase diagram. However, we think that the gross features and the qualitative trends are reproduced correctly. In

this section we only present our major results for the incoherent bcc/fcc phase diagram. Additional considerations for  $T \neq 0$ , also for the binary subsystems, can be found in [33,40].

We begin with a discussion of the ternary phase diagram computed at  $T=1250$  K as shown in Fig. 6. Starting at low Al concentration, there is a wide heterogeneous B2–A1 phase mixture stabilized up to 50% Al. Due to the low ordering energy in the upper half of the Gibbs triangle, there are only a few complicated single-phase structures with rather big unit cells ([23] and references therein). These structures can not be represented in the tetrahedron approximation, and thus are not considered in our investigation. A rather broad B2 phase is stabilized in the center of the Gibbs triangle. The other stable phases are also ternary extensions of the known stable binary phases. Remarkably, the B2 phase varies continuously from NiAl to FeAl, i.e., B2–NiAl and B2–FeAl are soluble into one another over a wide composition range. However, our calculations also reveal a miscibility gap (MG) within the ternary B2–(Ni,Fe)Al phase along the Fe–NiAl direction which is already known from experiments [22,41]. Our approach allows for the identification of the two different B2 phases involved in the MG. The first B2 phase is mainly oriented along NiAl–FeAl and can be defined by stating that the occupation of the Al sublattice of the B2 structure is strongly dominated by the Al atoms, whereas the substitution processes of Ni and Fe takes place solely via the transition metal sublattice. This type of microstructure was already found in our ground state calculations along NiAl–FeAl (section 3.1.3). The second B2 phase develops for higher Fe concentration along A2–Fe–B2–NiAl. There, the majority Fe atoms now also manifestly replace Al atoms on their sublattice, i.e., the Fe atoms are not anymore mainly restricted to the transition metal sublattice. The latter type of B2 phase obviously triggers the continuous B2–A2 transition towards the Fe corner. The location of the MG is close to the region where the overall stability of the parent bcc lattice is rather delicate (see Fig. 3b). Hence, the appearance of the MG may be related to the existing of the two distinct minima, i.e., one at the NiAl stoichiometry and the other in the Fe corner, in the formation energy landscape for homogeneous phases on the bcc parent lattice, as discussed in section 3.1.3. In connection to this it seems that by starting from B2–FeAl the sole transformation of the Fe sublattice into an Ni sublattice when going towards the NiAl stoichiometry, as well as the sole vanishing of the Al sublattice when going towards the Fe corner, can be accomplished continuously. In contrast, the system gets somehow “frustrated” when the two B2 sublattices have to be transformed simultaneously, as it happens when going along the FeAl–Ni line. Then it is thermodynamically more favourable to eventually open the MG and stabilize a heterogeneous mixture of two B2 phases. Finally, by continuing along the FeAl–Ni line this MG also breaks down and a full B2–A2 mixture becomes stable. Note that a “stoichiometric splitting”, i.e., the formation of two lines of stability for B2–(Ni,Fe)Al is also described in the experimental work of Tan *et al.* [42]. We think that the confirmation of the MG is a very big success of our ab-initio statistical

mechanics in view of the fact that it does not involve any fit parameter. The topology of the obtained ab-initio phase diagram at  $T=1250$  K matches nicely the one of the experimental phase diagram around 670 K published in the book of Sauthoff [9]. We want to remark on two specific problems concerning the latter comparison. First, due to the wrong stabilization of the  $L1_2$  structure instead of the  $D0_3$  structure for  $Fe_3Al$  at  $T=0K$  in PBE-GGA, the  $L1_2-Fe_3Al$  phase also appears as a stable phase in our calculated ternary phase diagram. Second, in nature fcc-Fe is stabilized against bcc-Fe at  $T=1250$  K. The corresponding allotropic transformation, mainly driven by phonons, can of course not be reproduced by our approach. The matching of our high- $T$  phase diagram with the experimental one at much lower temperatures may be due to the limitations of the tetrahedron approximation and the fact that DFT calculations often tend to overestimate the formation energy. Our phase diagram at 1250 K does not include the  $L1_2-Ni_3Fe$  phase although we have identified the corresponding configuration as a ground-state structure. This is due to the fact that the binary  $Ni_3Fe$  phase already disorders at 660 K in our CVM examinations of binary Ni-Fe [40], and it is surely not expected that a ternary continuation of  $Ni_3Fe$  leads to a tremendous increase of the order-disorder transition temperature  $T_{Ni_3Fe}^{(dis)}$ . Thus in order to investigate the phase stability of possible ternary  $Ni_3Fe$  we calculated the incoherent Ni-Fe-Al phase diagram also at 500 K (Fig. 7), but only in the Ni-Fe-NiAl triangle of the full Gibbs triangle. In addition to the already existing phases at 1250 K, indeed there is now also a  $Ni_3Fe$  phase with  $L1_2$  symmetry. Surprisingly, a ternary  $Ni_3Fe$  phase was not indicated in the experimental phase diagram around 670 K from Ref. [9], although the experimental value of  $T_{Ni_3Fe}^{(dis)}$  amounts up to 790 K [13]. In our calculation  $Ni_3Fe$  and  $Ni_3Al$  are well soluble into one another over a wide composition range, in analogy to the case of B2. Moreover, within the given approximations there is also a miscibility gap (MG) existing in this generic  $L1_2$  phase. Further calculations revealed that this  $L1_2$ -MG has vanished at 600 K, thus the MG should be confined to the low temperature regime. Experimental investigations to test these latter low temperature results are highly desirable.

### 3.3 Conclusions

In conclusion, we have presented a first-principles modelling of the technologically important Ni-Fe-Al system. The emphasis of our work is on the completeness of the description rather than on specific details of this complex ternary system. Hence, approximations, both on a physical and numerical level, had to be applied to render the approach feasible. Although some of these approximations surely have to be removed in detailed analyses of certain properties of Ni-Fe-Al, we think that our approach yields important information for an identification of the relevant physical processes and interactions that have



dominant influence in this intermetallic system. For instance, we have shown that the influence of magnetism is not negligible for a vast composition range. The atomic ordering in the ternary B2 phase is another interesting result, not only from the point of view of basic research but also concerning the manufacturing of new alloys with varying Fe content. Generally, in spite of the complexity of the problem, our rather simple approach yields encouraging agreement with the real Ni-Fe-Al system. Of course, more specialized theoretical and experimental work is needed. Thus, we hope to generally stimulate further research on this and other multicomponent intermetallic systems, since they provide a fascinating variety of interacting physical processes due to the enlarged number of degrees of freedom. After all, such systems are generally of higher technological relevance than the more restricted binary systems.

## Acknowledgements

This work was supported by the Deutsche Forschungsgemeinschaft (DFG) under the project No. FA 196/9-1.

## References

- [1] *Statics and Dynamics of Alloy Phase Transformations*, edited by P.E.A. Turchi and A. Gonis, NATO ASI Series B: Physics Vol. 319 (Plenum, New York, 1994).
- [2] P. Hohenberg and W. Kohn, Phys. Rev. 1964;136:B864.
- [3] W. Kohn and L.J. Sham, Phys. Rev. A 1965;140:1133.
- [4] J.M. Sanchez, F. Ducastelle and D. Gratias, Physica A 1984;128:334.
- [5] J.W.D. Connolly and A.R. Williams, Phys. Rev. B 1983;27:5169.
- [6] R. Kikuchi, Phys. Rev. 1951;81:988.
- [7] T. Morita, J. Phys. Soc. Jpn. 1957;12:753 , J. Math. Phys. 1972;13:115.
- [8] A. Finel, in Ref. [1], p. 495.
- [9] G. Sauthoff, *Intermetallics* (VCH, 1995) ; Intermetallics 2000;8:1101.
- [10] C.T. Liu and D.P. Pope, in *Intermetallic compounds – principles and practise*, edited by J.H. Westbrook and R.L. Fleischer (John Wiley & Sons, 1995).
- [11] R. Darolia, D. Lahrman and R. Field, Scripta metall. 1992;27:1795.
- [12] D. Letzig, J. Klöwer and G. Sauthoff, Zeitschrift für Metallkunde 1999;90:712.
- [13] L.J. Swartzendruber, V.P. Itkin and C.B. Alcock, J. Phase Equil. 1991;12:288.

- [14] P. Nash, M.F. Singelton and J.L. Murray, in *Phase Diagrams of Binary Nickel Alloys*, edited by P. Nash (ASM International Materials Park, OH, 1991).
- [15] U.R. Kattner and B.P. Burton, in *Phase Diagrams of Binary Iron Alloys*, edited by H. Okamoto (ASM International Materials Park, OH, 1993).
- [16] P. Entel, E. Hoffmann, P. Mohn, K. Schwarz and V.L. Moruzzi, *Phys. Rev. B* 1993;47:8706.
- [17] B.I. Min, T. Oguchi, H.J.F. Jansen, and A.J. Freeman, *J. Magn. Magn. Mater.* 1986;54-57:1091.
- [18] F. Lechermann, F. Welsch, C. Elsässer, C. Ederer, M. Fähnle, J.M. Sanchez and B. Meyer, *Phys. Rev. B* 2002;65:132104.
- [19] F. Lechermann, M. Fähnle, B. Meyer and C. Elsässer, *Phys. Rev. B* 2004;69:165116.
- [20] T. Shinoda, Y. Mishima, K. Masuda-Jindo, M.H.F. Sluiter, *J. Phase Equil.* 1997;18:624.
- [21] M. Enomoto, H. Harada, M. Yamazaki, *Calphad* 1991;15:143.
- [22] V.G. Rivlin and G.V. Raynor, *Int. Met. Rev.* 1980;25:79.
- [23] P. Budberg and A. Prince, in *Ternary Alloys*, edited by G. Petzow and G. Efferberg (VCH, 1992).
- [24] B. Meyer, C. Elsässer, F. Lechermann and M. Fähnle, *FORTRAN 90 Program for Mixed-Basis-Pseudopotential Calculations for Crystals*, Max-Planck-Institut für Metallforschung, Stuttgart, unpublished.
- [25] J.P. Perdew, K. Burke and M. Ernzerhof, *Phys. Rev. Lett.* 1996;77:3865, 1997;78:1396.
- [26] C. Wolverton and D. de Fontaine, *Phys. Rev. B* 1994;49:8627.
- [27] D. de Fontaine, in *Solid State Physics Vol. 47* edited by H. Ehrenreich and D. Turnbull (Academic Press, New Yprk, 1994).
- [28] G. Inden, in *Phase Transformations in Materials* edited by G. Kostorz (Wiley-VCH, 2001).
- [29] G.R. Caskey, J.M. Franz and D.J. Stellmyer, *J. Phys. Chem. Solids* 1973;34:1179.
- [30] C. Wolverton, *Modelling Simul. Mater. Sci. Eng.* 2000;8:323.
- [31] R. Kikuchi, *J. Chem. Phys.* 1974;60:1071.
- [32] C. Colinet, G. Inden and R. Kikuchi, *Acta metall. mater.* 1993;41:1109.
- [33] F. Lechermann and M. Fähnle, *Phys. Rev. B* 2001;63:012104, *phys. status solidi B* 2001;224:R4.

- [34] R.E. Watson, M. Weinert and M. Alatalo, Phys. Rev. B 1998;57:12134.
- [35] M. van Schilfgaarde, I.A. Abrikosov and B. Johansson, Nature 1999;400:46.
- [36] M. Sluiter, P.E.A. Turchi, F.J. Pinski, and G.M. Stocks, Mater. Sci. Eng. A 1992;152:1.
- [37] C. Wolverton and A. Zunger, Phys. Rev. B 1999;59:12165.
- [38] J. Bogner, W. Steiner, M. Reissner, P. Mohn, P. Blaha, K. Schwarz, R. Krachler, H. Ipser and B. Sepiol, Phys. Rev. B 1998;58:14922.
- [39] C.S. Lue, Y. Oner, D.G. Naugle and J.H. Ross, Phys. Rev. B 2001;63:184405.
- [40] F. Lechermann, Ph.D. thesis, [elib.uni-stuttgart.de/opus/volltexte/2004/1601/](http://elib.uni-stuttgart.de/opus/volltexte/2004/1601/), University of Stuttgart (2003).
- [41] C.T. Liu, S.C. Jeng, and C.C. Wu, Metall. Mater. Trans. A 1992;23:1395.
- [42] Y. Tan, T. Shinoda, Y. Mishima, and T. Suzuki, Mat. Trans. 2001;42:464.

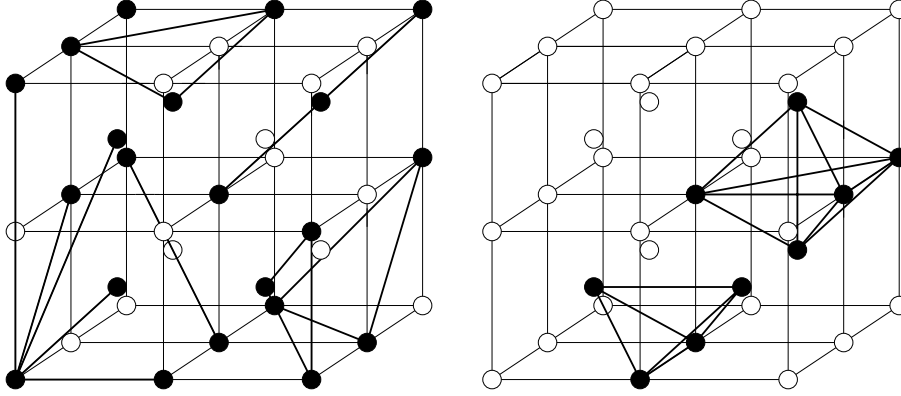


Fig. 1. Cluster used for the pentahedron approximation on the bcc lattice.

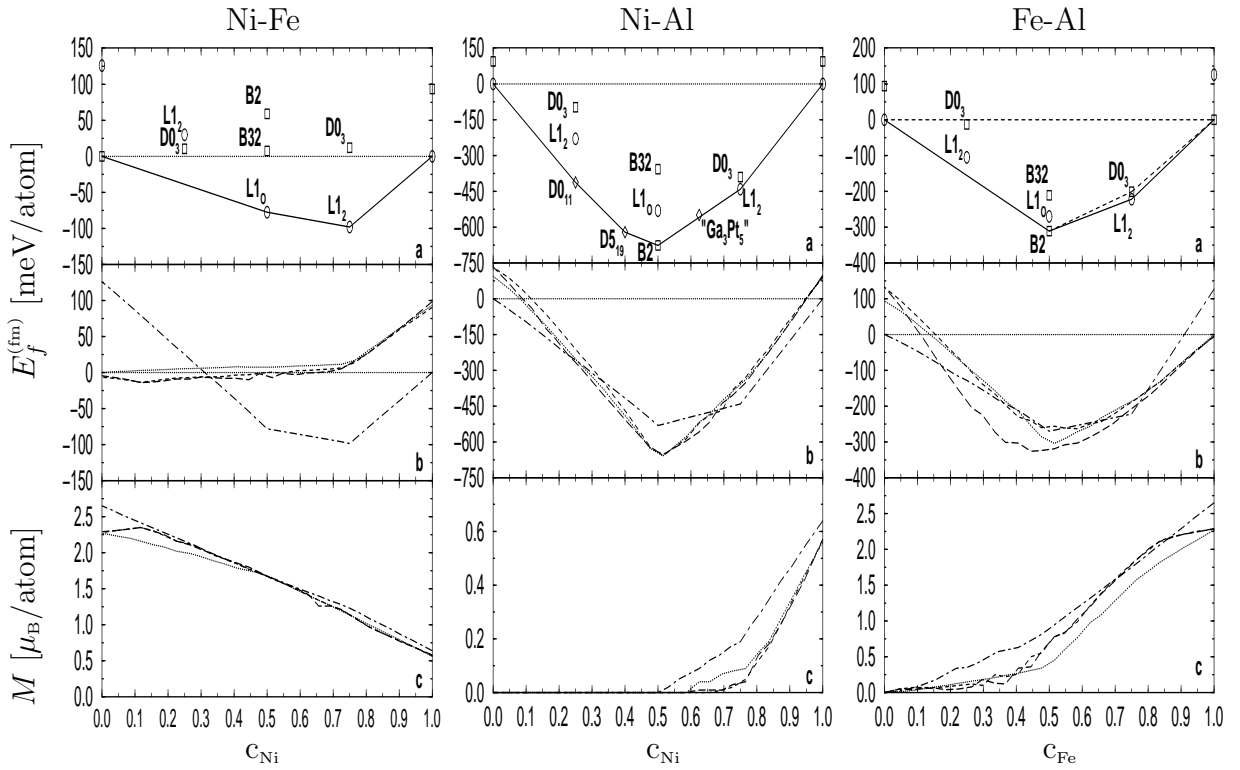


Fig. 2. Formation energy  $E_f^{(\text{fm})}$  and magnetic moment  $M$  in the binary systems Ni-Fe, Ni-Al and Fe-Al. (a)  $E_f^{(\text{fm})}$  according to the spin-polarized MBPP calculations. (b)  $E_f^{(\text{fm})}$  according to the constructed CEs. (c)  $M$  according to the constructed CEs. In (b) and (c) the dotted lines correspond to the bcc T-CE, dashed lines to the bcc P-CE, long-dashed lines to the bcc rP-CE and dotted-dashed lines to the fcc T-CE.

| structure                             | $a_{eq}$ [Å] | $B$ [Mbar] | $E_f$ [ $\frac{\text{meV}}{\text{atom}}$ ] | $M$ [ $\mu_B$ ] |
|---------------------------------------|--------------|------------|--|-----------------|
| bcc-Ni                                | 2.812        | 1.891      | 119.6                                      | 0.56            |
|                                       | 2.821        | 1.825      | 93.5                                       |                 |
| bcc-Fe*                               | 2.782        | 2.666      | 596.2                                      | 2.27            |
|                                       | 2.864        | 1.595      | 0.0  |                 |
| bcc-Al                                | 3.230        | 0.677      | 93.7                                       | 0.00            |
|                                       | 3.230        | 0.677      | 93.7                                       |                 |
| B2-NiFe                               | 2.797        | 2.214      | 445.7                                      | 3.58            |
|                                       | 2.877        | 1.673      | 58.6                                       |                 |
| B2-NiAl*                              | 2.898        | 1.546      | -676.8                                     | 0.00            |
|                                       | 2.898        | 1.546      | -676.8                                     |                 |
| B2-FeAl*                              | 2.872        | 1.762      | -288.7                                     | 0.73            |
|                                       | 2.879        | 1.550      | -311.3                                     |                 |
| B32-Ni <sub>2</sub> Fe <sub>2</sub>   | 2.797        | 2.254      | 413.4                                      | 6.70            |
|                                       | 2.859        | 1.755      | 7.2  |                 |
| B32-Ni <sub>2</sub> Al <sub>2</sub>   | 2.929        | 1.433      | -357.3                                     | 0.00            |
|                                       | 2.929        | 1.433      | -357.3                                     |                 |
| B32-Fe <sub>2</sub> Al <sub>2</sub>   | 2.899        | 1.698      | 20.8                                       | 3.95            |
|                                       | 2.941        | 1.406      | -211.6                                     |                 |
| D0 <sub>3</sub> -Ni <sub>3</sub> Fe   | 2.806        | 2.053      | 307.7                                      | 4.56            |
|                                       | 2.842        | 1.813      | 11.9                                       |                 |
| D0 <sub>3</sub> -NiFe <sub>3</sub>    | 2.789        | 2.445      | 521.9                                      | 8.85            |
|                                       | 2.882        | 1.738      | 10.1                                       |                 |
| D0 <sub>3</sub> -Ni <sub>3</sub> Al   | 2.847        | 1.740      | -389.9                                     | 0.00            |
|                                       | 2.847        | 1.740      | -389.9                                     |                 |
| D0 <sub>3</sub> -NiAl <sub>3</sub>    | 3.059        | 1.013      | -97.7                                      | 0.00            |
|                                       | 3.059        | 1.013      | -97.7                                      |                 |
| D0 <sub>3</sub> -Fe <sub>3</sub> Al*  | 2.821        | 2.181      | 106.1                                      | 6.35            |
|                                       | 2.892        | 1.510      | -201.0                                     |                 |
| D0 <sub>3</sub> -FeAl <sub>3</sub>    | 2.990        | 1.274      | -13.1                                      | 0.00            |
|                                       | 2.989        | 1.196      | -13.1                                      |                 |
| L2 <sub>1</sub> -Ni <sub>2</sub> FeAl | 2.850        | 1.836      | -98.7                                      | 3.39            |
|                                       | 2.886        | 1.631      | -345.4                                     |                 |
| L2 <sub>1</sub> -NiFe <sub>2</sub> Al | 2.834        | 1.991      | 46.9                                       | 4.88            |
|                                       | 2.890        | 1.437      | -98.6                                      |                 |
| L2 <sub>1</sub> -NiFeAl <sub>2</sub>  | 2.878        | 1.662      | -492.2                                     | 0.36            |
|                                       | 2.881        | 1.492      | -494.3                                     |                 |
| F $\bar{4}$ 3m-Ni <sub>2</sub> FeAl   | 2.844        | 1.847      | -130.0                                     | 2.88            |
|                                       | 2.869        | 1.635      | -279.2                                     |                 |
| F $\bar{4}$ 3m-NiFe <sub>2</sub> Al   | 2.834        | 2.011      | 1.7  | 4.90            |
|                                       | 2.883        | 1.677      | -299.8                                     |                 |
| F $\bar{4}$ 3m-NiFeAl <sub>2</sub>    | 2.918        | 1.545      | 21 -120.9                                  | 2.26            |
|                                       | 2.956        | 1.276      | -178.7                                     |                 |

Table 1

Structural data for the bcc structures used in the SIM for the tetrahedron approx-

| structure                            | $a_{eq}$ [Å] | $B$ [Mbar] | $E_f$ [ $\frac{\text{meV}}{\text{atom}}$ ] | $M$ [ $\mu_B$ ] |
|--------------------------------------|--------------|------------|--|-----------------|
| fcc-Ni*                              | 3.536        | 1.940      | 65.9                                       | 0.64            |
|                                      | 3.544        | 1.892      | 0.0  |                 |
| fcc-Fe                               | 3.478        | 2.790      | 286.2                                      | 2.65            |
|                                      | 3.668        | 1.643      | 125.6                                      |                 |
| fcc-Al*                              | 4.036        | 0.755      | 0.0  | 0.00            |
|                                      | 4.036        | 0.755      | 0.0  |                 |
| L1 <sub>0</sub> -NiFe                | 3.509        | 2.320      | 287.9                                      | 6.69            |
|                                      | 3.594        | 1.788      | -77.8                                      |                 |
| L1 <sub>0</sub> -NiAl                | 3.671        | 1.492      | -531.1                                     | 0.00            |
|                                      | 3.671        | 1.492      | -531.1                                     |                 |
| L1 <sub>0</sub> -FeAl                | 3.659        | 1.700      | -69.6                                      | 3.54            |
|                                      | 3.704        | 1.391      | -270.3                                     |                 |
| L1 <sub>2</sub> -Ni <sub>3</sub> Fe* | 3.524        | 2.117      | 214.5                                      | 4.91            |
|                                      | 3.571        | 1.864      | -98.3                                      |                 |
| L1 <sub>2</sub> -NiFe <sub>3</sub>   | 3.493        | 2.543      | 310.4                                      | 8.56            |
|                                      | 3.630        | 1.523      | 29.8                                       |                 |
| L1 <sub>2</sub> -Ni <sub>3</sub> Al* | 3.581        | 1.763      | -434.8                                     | 0.74            |
|                                      | 3.582        | 1.757      | -441.0                                     |                 |
| L1 <sub>2</sub> -NiAl <sub>3</sub>   | 3.843        | 1.100      | -230.0                                     | 0.00            |
|                                      | 3.843        | 1.100      | -230.0                                     |                 |
| L1 <sub>2</sub> -Fe <sub>3</sub> Al  | 3.567        | 2.137      | 174.3                                      | 6.99            |
|                                      | 3.669        | 1.680      | -222.0                                     |                 |
| L1 <sub>2</sub> -FeAl <sub>3</sub>   | 3.793        | 1.275      | -105.3                                     | 0.26            |
|                                      | 3.797        | 0.988      | -105.3                                     |                 |
| P4/mmm-Ni <sub>2</sub> FeAl          | 3.581        | 1.865      | -158.5                                     | 3.00            |
|                                      | 3.617        | 1.664      | -325.1                                     |                 |
| P4/mmm-NiFe <sub>2</sub> Al          | 3.573        | 2.004      | 17.5                                       | 5.08            |
|                                      | 3.646        | 1.626      | -263.7                                     |                 |
| P4/mmm-NiFeAl <sub>2</sub>           | 3.664        | 1.598      | -309.6                                     | 1.78            |
|                                      | 3.691        | 1.414      | -392.5                                     |                 |

Table 2

Structural data for the fcc structures used in the SIM for the tetrahedron approximation (see text).

| cluster $\alpha$ | bcc                   |                       |                       |                       | fcc                   |                       |                       |                       |
|------------------|-----------------------|-----------------------|-----------------------|-----------------------|-----------------------|-----------------------|-----------------------|-----------------------|
|                  | $\Theta_2$            |                       | $\Theta_1$            |                       | $\Theta_2$            |                       | $\Theta_1$            |                       |
|                  | $K_{\alpha m}^{(nm)}$ | $K_{\alpha m}^{(fm)}$ | $K_{\alpha m}^{(nm)}$ | $K_{\alpha m}^{(fm)}$ | $K_{\alpha m}^{(nm)}$ | $K_{\alpha m}^{(fm)}$ | $K_{\alpha m}^{(nm)}$ | $K_{\alpha m}^{(fm)}$ |
| empty            | -29.0                 | -203.1                | 93.7                  | 93.7                  | -89.1                 | -261.6                | 0.0                   | 0.0                   |
| point            |                       |                       |                       |                       |                       |                       |                       |                       |
| 1                | -243.8                | -85.7                 | -169.2                | -169.2                | -258.7                | -128.8                | -249.4                | -249.4                |
| 2                | -330.3                | -81.4                 | -596.4                | -596.4                | -308.4                | -118.4                | -670.6                | -670.6                |
| NN pair          |                       |                       |                       |                       |                       |                       |                       |                       |
| 11               | -13.6                 | -9.8                  | -23.7                 | -52.9                 | -8.2                  | 2.2                   | 4.6                   | -4.1                  |
| 12               | -9.5                  | -35.9                 | -104.5                | 11.8                  | -26.1                 | -13.9                 | -106.1                | -5.7                  |
| 22               | 92.1                  | 71.8                  | 59.9                  | -27.1                 | 48.5                  | 47.3                  | 30.3                  | -61.3                 |
| NNN pair         |                       |                       |                       |                       |                       |                       |                       |                       |
| 11               | -2.3                  | 5.3                   | 3.2                   | 0.1                   | -                     | -                     | -                     | -                     |
| 12               | -4.7                  | 8.4                   | -73.0                 | -65.4                 | -                     | -                     | -                     | -                     |
| 22               | 10.6                  | 8.9                   | -188.7                | -193.1                | -                     | -                     | -                     | -                     |
| triangle         |                       |                       |                       |                       |                       |                       |                       |                       |
| 111              | -1.0                  | 0.8                   | -3.6                  | 0.7                   | -1.2                  | 1.1                   | -5.1                  | -2.2                  |
| 112              | -2.1                  | -4.8                  | -3.6                  | 23.0                  | 2.8                   | -7.6                  | -29.3                 | -7.8                  |
| 121              | 0.0                   | -0.3                  | -4.9                  | 5.1                   | -                     | -                     | -                     | -                     |
| 122              | 3.3                   | 2.2                   | 46.0                  | 20.7                  | 16.4                  | -0.4                  | 105.4                 | 49.5                  |
| 212              | 1.7                   | 1.8                   | 23.3                  | 14.3                  | -                     | -                     | -                     | -                     |
| 222              | -3.1                  | -3.6                  | 147.6                 | 141.1                 | 2.3                   | -1.5                  | 163.3                 | 191.6                 |
| tetrahedron      |                       |                       |                       |                       |                       |                       |                       |                       |
| 1111             | -0.3                  | 0.7                   | -0.6                  | 1.6                   | -0.3                  | -0.9                  | -0.6                  | -2.1                  |
| 1112             | -1.3                  | -0.6                  | 5.2                   | 2.4                   | -4.3                  | -6.4                  | 16.7                  | 25.0                  |
| 1122             | 2.3                   | -1.7                  | 15.6                  | -11.8                 | 9.1                   | 14.2                  | 61.6                  | 96.1                  |
| 1212             | 1.1                   | -1.0                  | 7.2                   | -6.4                  | -                     | -                     | -                     | -                     |
| 1222             | 3.6                   | 1.1                   | -42.1                 | -12.9                 | 2.6                   | 8.9                   | -30.2                 | -103.9                |
| 2222             | -4.4                  | -4.0                  | -88.4                 | -80.4                 | -13.7                 | -13.2                 | -278.2                | -266.4                |

Table 3

Ternary CE of the formation energy in tetrahedron approximation. ECIs  $K_{\alpha m}$  in meV/atom.

| EPI              | bcc   |       | fcc   |      |
|------------------|-------|-------|-------|------|
|                  | nm    | fm    | nm    | fm   |
| $W_{NiFe}^{(1)}$ | -20.4 | -14.7 | -12.3 | 3.3  |
| $W_{NiFe}^{(2)}$ | -3.5  | 8.0   | -     | -    |
| $W_{NiAl}^{(1)}$ | 110.9 | 123.7 | 85.4  | 72.1 |
| $W_{NiAl}^{(2)}$ | 17.2  | 1.1   | -     | -    |
| $W_{FeAl}^{(1)}$ | 86.2  | 30.5  | 17.6  | 36.0 |
| $W_{FeAl}^{(2)}$ | 5.0   | 22.9  | -     | -    |

Table 4

Effective quasibinary pair interactions in the Ni-Fe-Al system (in meV/atom).

| structure       | $a$ [a.u.] | $B$ [Mbar] | $E_{form}$ $\left[\frac{\text{meV}}{\text{atom}}\right]$ |        |        | $M$ [ $\mu_B$ ] |      |       |
|-----------------|------------|------------|--|--------|--------|-----------------|------|-------|
|                 |            |            | MBPP   | P-CE   | rP-CE  | MBPP            | P-CE | rP-CE |
| L2 <sub>1</sub> | 5.445      | 1.492      | -494.3   | -494.3 | -494.3 | 0.36            | 0.36 | 0.36  |
| G1              | 5.443      | 1.586      | -519.4   | -503.2 | -517.4 | 0.00            | 0.36 | 0.16  |
| G2              | 5.433      | 1.530      | -528.8   | -523.9 | -524.2 | 0.00            | 0.48 | 0.48  |
| NiAl–FeAl       |            |            | -494.1   |        |        |                 |      |       |

Table 5

Structural data for the competing structures at NiFeAl<sub>2</sub>. The MBPP value  $E_f^{(fm)}$  for the G2 structure belongs to the structurally relaxed geometry.



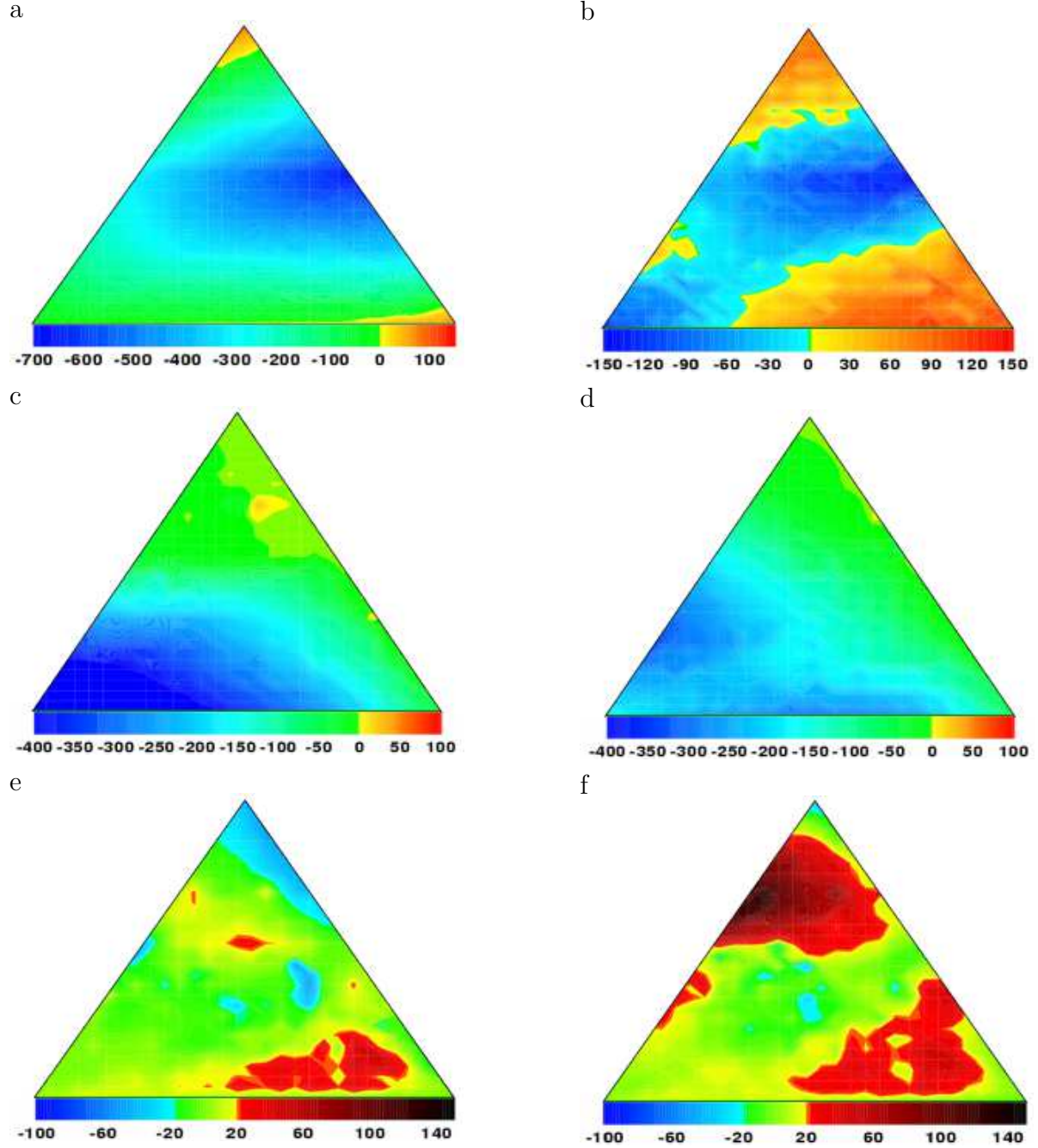


Fig. 3. Ternary formation energies  $E_f^{(\text{fm})}$  and differences  $\Delta E_f$  (in meV/atom). The Gibbs triangle is oriented with the Al corner at the top, Fe corner on the left and Ni corner on the right. All energies in the series (a)-(d) belong to the CEs in tetrahedron approximation. (a)  $E_f^{(\text{fm})}$  on the bcc lattice. (b)  $\Delta E_f^{(\text{fm})}(\text{bcc-fcc})$  between the formation energy on the bcc and fcc lattice. (c)  $\Delta E_f^{(\text{fm})-(\text{nm})}(\text{bcc})$  between the fm and nm formation energy on the bcc lattice. (d)  $\Delta E_f^{(\text{fm})-(\text{nm})}(\text{fcc})$  between the fm and nm formation energy on the fcc lattice. (e) Difference between  $E_f^{(\text{fm})}(\text{bcc})$  in tetrahedron and pentahedron approximation. (f) Difference between  $E_f^{(\text{fm})}(\text{bcc})$  in tetrahedron and relaxed pentahedron (rP-CE) approximation.

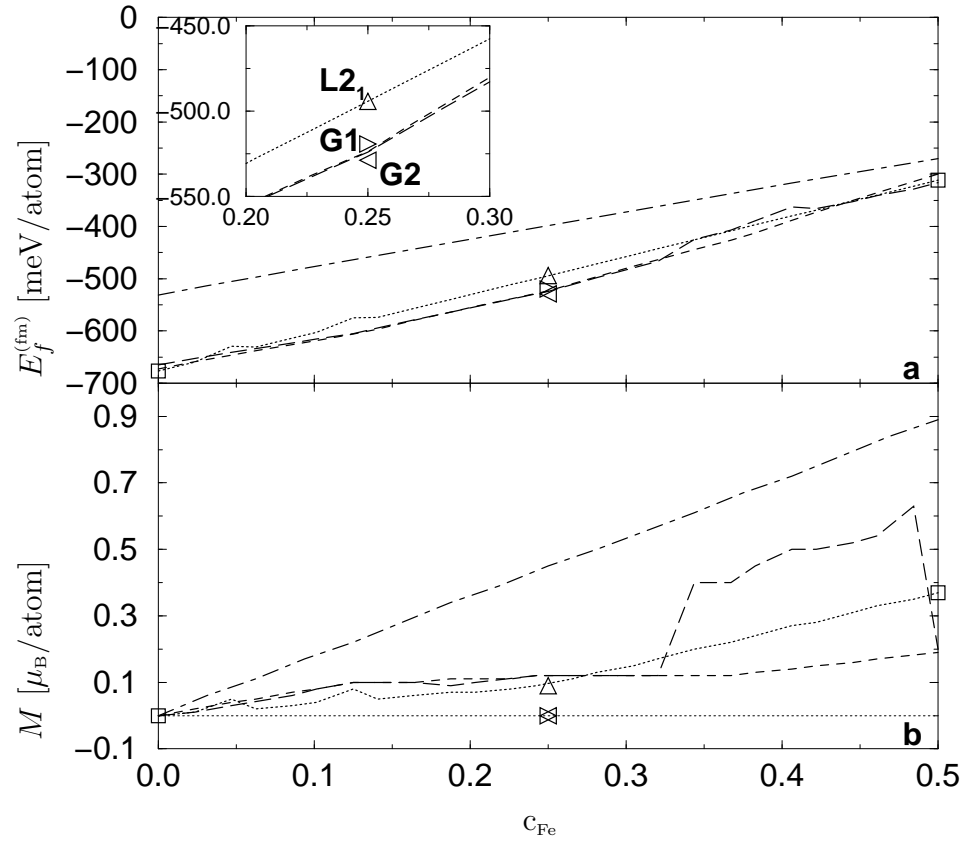


Fig. 4. Formation energy  $E_f^{(\text{fm})}$  (a) and magnetic moment  $M$  (b) along the NiAl–FeAl line in the Ni–Fe–Al Gibbs triangle. Symbols denote the MBPP values for the ordered structures. Lines are according to Fig. 2.

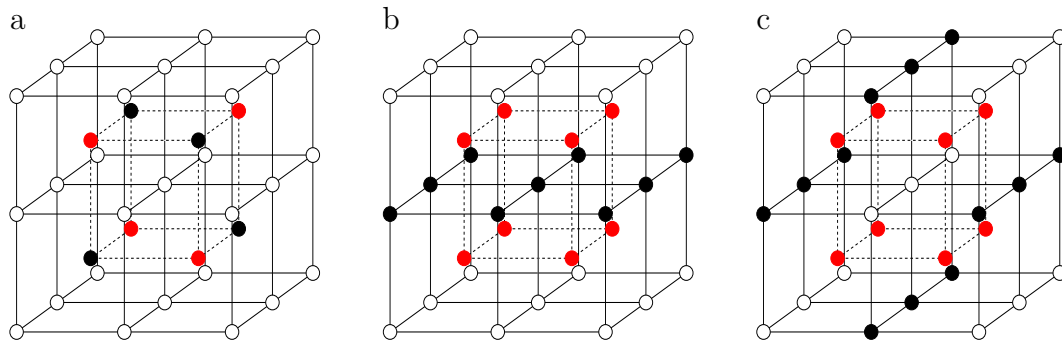


Fig. 5. Important ordered structures at  $\text{NiFeAl}_2$ . (a) L2<sub>1</sub>, (b) G1 and (c) G2. Open circles denote the Ni atoms, black circles the Fe atoms and (red/grey) circles the Al atoms.

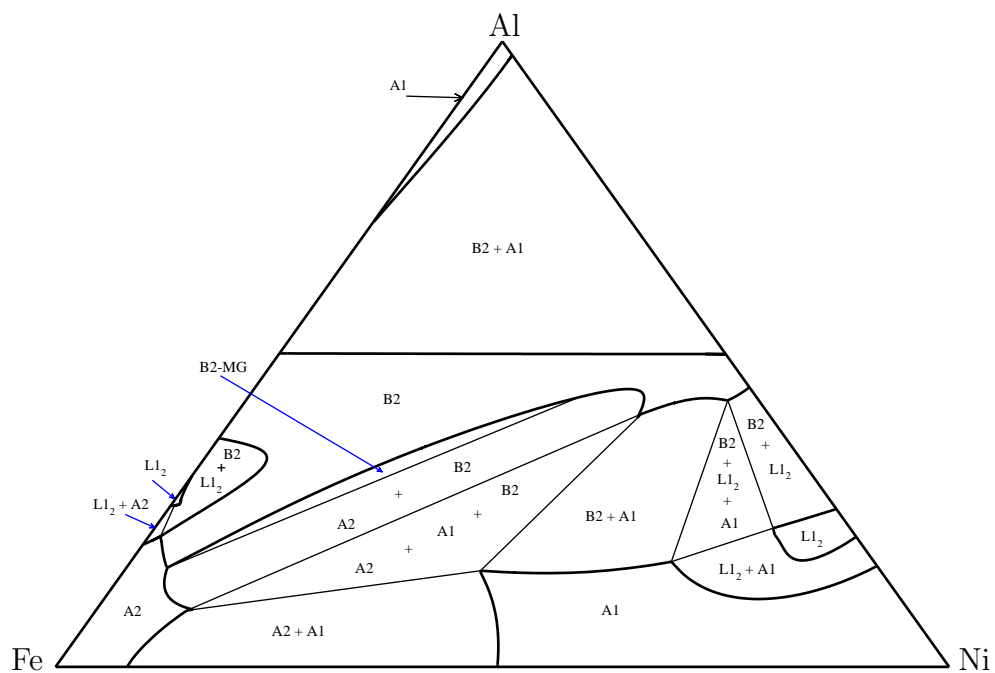


Fig. 6. Incoherent ab-initio phase diagram of Ni-Fe-Al on the bcc and fcc lattice. Computed with the tetrahedron approximation to the CVM at  $T=1250$  K.

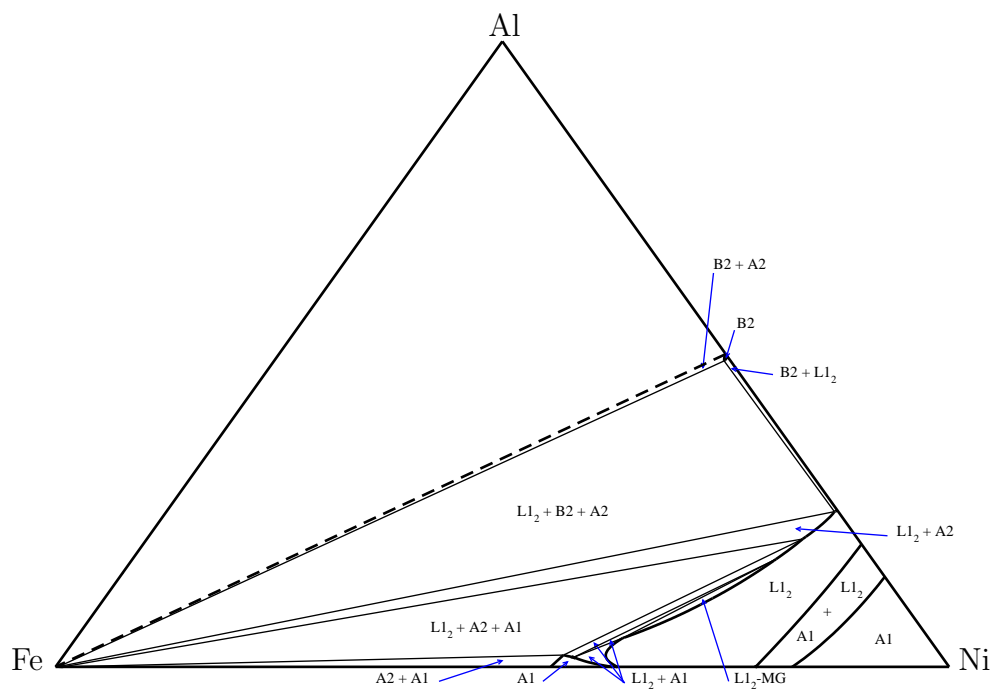


Fig. 7. Incoherent ab-initio phase diagram of Ni-Fe-Al on the bcc and fcc lattice. Computed with the tetrahedron approximation to the CVM at  $T=500$  K.